Available free online at www.medjchem.com

Mediterranean Journal of Chemistry

*Mediterranean Journal of Chemistry* **2020**, 10(8), 734-743

# Structure, Infrared and Raman spectroscopic studies of new $A^{II}(Sb^{V}_{0.50}Cr^{III}_{0.50})(PO_4)_2$ (A = Ba, Sr, Pb) yavapaiite phases

**Hajar Bellefqih, Rachid Fakhreddine, Rachid Tigha and Abderrahim Aatiq** *

University Hassan II of Casablanca, Faculty of Sciences Ben M'Sik, Chemistry Department. Laboratory of Physical-Chemistry of Applied Materials, Avenue Idriss El Harti, Po Box. 7955, Casablanca, Morocco

**Abstract**: Three new $A^{II}(Sb_{0.5}Cr_{0.5})(PO_4)_2$ ($A^{II}$ = Ba, Sr, Pb) yavapaiite phases, abbreviated as [ASbCr], have been successfully synthesized by a conventional solid-state reaction in air atmosphere. Their crystal structures have been investigated by Rietveld analysis from the X-ray powder diffraction method. Results show that $Ba(Sb_{0.5}Cr_{0.5})(PO_4)_2$ crystallizes in monoclinic *C2/m* space group (Z = 2) with cell parameters a = 8.140(1) Å; b = 5.175(1) Å; c = 7.802(1) Å and β = 94.387(1)°. Structures of $A^{II}(Sb_{0.5}Cr_{0.5})(PO_4)_2$ ($A^{II}$ = Sr, Pb) compounds are comparable, and both crystallize in a distorted yavapaiite structure with *C2/c* space group (Z = 4). Obtained monoclinic cell parameters are: a = 16.5038(2) Å; b = 5.1632(1) Å; c = 8.0410(1) Å; β = 115.85(1) for [SrSbCr] and a = 16.684(2) Å; b = 5.156(1) Å c = 8.115(1) Å; β = 115.35(1)° for [PbSbCr]. Infrared and Raman spectroscopic study was undertaken to provide information about vibrations bonds within the studied yavapaiite materials.

**Keywords**: Rietveld Refinements analysis; X-ray powder diffraction; Yavapaiite structure; Infrared and Raman spectroscopy.

## 1. Introduction

Phosphates with general $A^{II}M^{IV}(PO_4)_2$ formula have attracted significant attention for several decades due to their optical [1-5], magnetic [6], and dielectric properties [7]. Furthermore, they have also proved attractive as potential candidates for the immobilization of tetravalent actinides [8–11]. Therefore, it becomes of prime importance to investigate their crystal structure. Note that the nature and/or size of $A^{II}$ and $M^{IV}$ cations have a significant effect on the crystal structure of $A^{II}M^{IV}(PO_4)_2$ phases, and this has prompted many researchers to build a relationship between the composition and the crystal structure of certain compounds [12,13]. The larger $A^{II}$ cation can cause structural distortions, and more particularly, rotation of the $PO_4$ tetrahedra. This last phenomenon leads to the synthesis of new families of phases whose structures are linked to each other's [12–28]. Among these families, the attracted $A^{II}M^{IV}(PO_4)_2$ yavapaiite-type phases have a structure consisting of layers of $A^{II}$ ions in tenfold coordination alternating with dense slabs of $M^{IV}O_6$ and $PO_4$ polyhedra. Several derivatives have been observed, at room temperature, for the structure above type. It has been reported that in the case where the ionic radius of $M^{IV}$ shifts slightly towards high values, like in $Ba^{II}M^{IV}(PO_4)_2$ ($M^{IV}$ = Np, U, Th) [29,30], a super-yavapaiite, with a structure similar to the archetype $RbEu(SO_4)_2$ [31] (space group *C2/c*, Z=4), is formed. Such a structure-type is made of layers of $Ba^{II}O_{14}$ polyhedra alternating with dense slabs of $M^{IV}O_8$ square-based antiprisms and $PO_4$ tetrahedra. The high coordination of $Ba^{II}$ and $M^{IV}$ ($M^{IV}$ = Np, U, Th) ions was shown to be consistent with their large size. For small $A^{II}$ and $M^{IV}$ cations, as in the case of $SrM^{IV}(PO_4)_2$ ($M^{IV}$ = Ge, Ti, Sn) [20,24] and $PbM^{IV}(PO_4)_2$ ($M^{IV}$ = Ge and Ti) [2], a distorted yavapaiite structure-type with *C2/c* space group (Z=4) was reported. This latter structure has a double lattice along the a-axis. Compared to the true-yavapaiite type, the $M^{IV}$ cation remains in octahedral polyhedral, whereas the $A^{II}$ cation coordination decreases to eight capped with two supplemental oxygen ions. The $PbSn(PO_4)_2$ structure crystallizes in the $P2_1/n$ space group under noncompact yavapaiite form with a $[Sn(PO_4)_2]^{2-}$ skeleton built of corner-linked $SnO_6$ octahedra and $PO_4$ tetrahedra. In contrast, the $Pb^{II}$ cations are distributed in double tunnels in place of sheets [22]. On the other hand, $SrM^{IV}(PO_4)_2$ ($M^{IV}$ = Np, U) was described as a modified cheralite structure (*Cmca* space group, Z=8) [30,32].

The main aim of our present work is to investigate the possibility of synthesizing numerous compounds in which the transition metal exhibits a reduced

*Corresponding author: Abderrahim Aatiq
Email address: a_aatiq @yahoo.fr
DOI: http://dx.doi.org/10.13171/mjc10802108201448hb

Received April 15, 2020
Accepted June 15, 2020
Published August 21, 2020

oxidation state. As a result of our investigation, $A^{II}(Sb^{V}_{0.5}Fe^{III}_{0.5})(PO_4)_2$ ($A^{II}$ = Sr, Pb, Ba) [33] and $Ba^{II}(Nb^{V}_{0.5}M^{III}_{0.5})(PO_4)_2$ ($M^{III}$ = Al, Cr, Fe, In) [34] compounds have been synthesized and characterized by some of us. The crystal structure of $Ba^{II}(Sb^{V}_{0.5}Fe^{III}_{0.5})(PO_4)_2$ and $Ba^{II}(Nb^{V}_{0.5}M^{III}_{0.5})(PO_4)_2$ belongs to the true-yavapaiite structure (*C2/m* space group, Z = 2). In contrast, $A^{II}(Sb^{V}_{0.5}Fe^{III}_{0.5})(PO_4)_2$ ($A^{II}$ = Sr, Pb) compounds exhibit a distorted yavapaiite structure type with *C2/c* space group (Z = 4). So, in a continuation of our scientific search, we synthesized new $A^{II}Sb^{V}_{0.5}Cr^{III}_{0.5}(PO_4)_2$ ($A^{II}$ = Sr, Pb, Ba) yavapaiite phases. The obtained materials have been structurally characterized by using X-ray powder diffraction. In order to get further structural information about the nature of bonding in the crystalline solids, Infrared and Raman spectroscopic study of selected phases is also presented.

## 2. Experimental

$A^{II}(Sb_{0.5}Cr_{0.5})(PO_4)_2$ ($A^{II}$= Ba, Sr, Pb) materials were prepared by conventional solid-state reaction from stoichiometric amounts of carbonates $SrCO_3$ (Riedel-de Haën, 99%), $BaCO_3$ (Riedel-de Haën, 99%) or nitrates $Pb(NO_3)_2$ (Prolabo, 99%), $Cr_2O_3$ (Prolabo, 99%), $Sb_2O_3$ (Riedel-de Haën, 99.9%), $NH_4H_2PO_4$ (Riedel-de Haën, 99%). Powders were mixed and ground and then heated in an air atmosphere between 200 and 750°C. To obtain a pure sample, a final treatment at 800°C for 48 hours, with periodic intermediate regrinding, is necessary.

X-ray powder diffraction data (XRPD) for $A^{II}(Sb_{0.5}Cr_{0.5})(PO_4)_2$ ($A^{II}$ = Ba, Sr, Pb) were collected, at room temperature, on X-Ray diffractometer (PANalytical X'Pert Pro) using monochromatized CuKα radiation (50 kV, 40 mA). The patterns were scanned in the 10-90° $2\theta$ range with a counting time of 30 *s* per step. The full pattern refinements were performed by the Rietveld refinement method with the aid of FullProf program [35] embedded in WinPlotr software [36]. A pseudo-Voigt function described the peak shape, and the background level was modeled by linear interpolation. The refined parameters were: scale factor, zero shift, lattice constants, peak profile, asymmetry parameters, atomic positions, and independent isotropic atomic displacement parameters. Infrared spectroscopic analyses were performed using a Bruker's VERTEX 70 spectrometer. All measurements were performed at room temperature. Raman scattering spectra were recorded on powder with a HORIBA, LabRAM HR Evolution spectrometer, equipped with an ionized argon laser. The finely ground substance is spread on a glass slide. The electrodes were illuminated with a 532 nm beam in ambient air.

## 3. Results and Discussion

### 3.1. Rietveld refinement and structural description of $Ba(Sb_{0.5}Cr_{0.5})(PO_4)_2$

According to the literature data, most barium orthophosphate compounds have been mentioned as entirely isotypic with true-yavapaiite (T.Y). Analysis of the powder XRD pattern using the Rietveld refinement in Le Bail's of [BaSbCr] phase revealed the presence of a crystallized phase exhibiting peak positions lines that match with $Ba(Sb_{0.5}Fe_{0.5})(PO_4)_2$ monoclinic phase [33]. Thus, starting structural parameters for the Rietveld refinement were taken from the true-yavapaiite phase mentioned above [33]. This refinement yielded to acceptable reliability factors (i.e., $R_{WP}$ = 8.9%; $R_P$ = 6.4%; $R_B$ = 3.7%; $R_F$ = 2.5%). The main refined parameters are given in Table 1. Observed, calculated, and difference XRD patterns of [BaSbCr] phase are presented in Figure 1.

**Table 1.** Crystallographic data of $Ba(Sb_{0.5}Cr_{0.5})(PO_4)_2$ (*C2/m* space group, Z =2).

**$BaSb_{0.5}Cr_{0.5}(PO_4)_2$**

Space group, *C2/m* (N°12); [Z = 2; a= 8.140(1) Å; b= 5.175(1) Å c= 7.802(1) Å; β = 94. 387(1) °; V = 328(1) $Å^3$]
Experimental data
Temperature, 25°C; angular range, 10° ≤ $2\theta$ ≤ 90°
step scan increment ($2\theta$) : 0.01671°
Zero-point ($2\theta$), -0.015(1)°
Profile parameters
Pseudo-Voigt function, PV = ηL + (1-η)G; η = 0.435(6)
Half-width parameters, U = 0.392 (4), V = -0.177 (3), and W = 0.0365 (1)
Conventional Rietveld R-factors, $R_{WP}$ = 8.9%; $R_P$ = 6.4%; $R_B$ = 3.7%; $R_F$ = 2.5%

| Atom | Site | Wyckoff positions | | | $B_{iso}$(Å$^2$) | Occupancy |
|---|---|---|---|---|---|---|
| **Ba** | 2c | 0 | 0 | 0.5 | 2.1(1) | 1 |
| **Sb(Cr)** | 2a | 0 | 0 | 0 | 2.0(5) | 0.5/0.5 |
| **P** | 4i | 0.3672(2) | 0 | 0.2014(3) | 2.1(5) | 1 |
| **O(1)** | 4i | 0.2384(6) | 0 | 0.0503(4) | 1.2(1) | 1 |
| **O(2)** | 4i | 0.3050(6) | 0 | 0.3867(6) | 1.2(1) | 1 |
| **O(3)** | 8j | 0.4761(5) | 0.2483(5) | 0.1862(5) | 1.2(1) | 1 |

The crystal structure of $Ba(Sb_{0.5}Cr_{0.5})(PO_4)_2$ can be described as made of layers of $Ba^{II}$ cations in tenfold coordination, alternating with dense slabs built up of corner-connected of $M^{IV}O_6$ octahedra and $PO_4$ tetrahedra (Figure 2). Note that each $PO_4$ tetrahedron presents one free oxygen pointing out of the layer. $Sb^{V}$ and $Cr^{III}$ cations are octahedrally surrounded by six oxygen atoms belonging to six $PO_4$ groups to form $Sb(Cr)O_6$ octahedral geometry. Reciprocally, each $PO_4$ tetrahedra is connected to three $Sb(Cr)O_6$ octahedra via vertex-sharing oxygen atoms. Oxygen atoms tenfold coordinate the BaII cation from eight bidentate $PO_4$ groups, and the other two oxygen atoms belong to the two other unidentate $PO_4$ groups. The $BaO_{10}$ is linked to six other $BaO_{10}$ adjacent polyhedra via edges and corners.

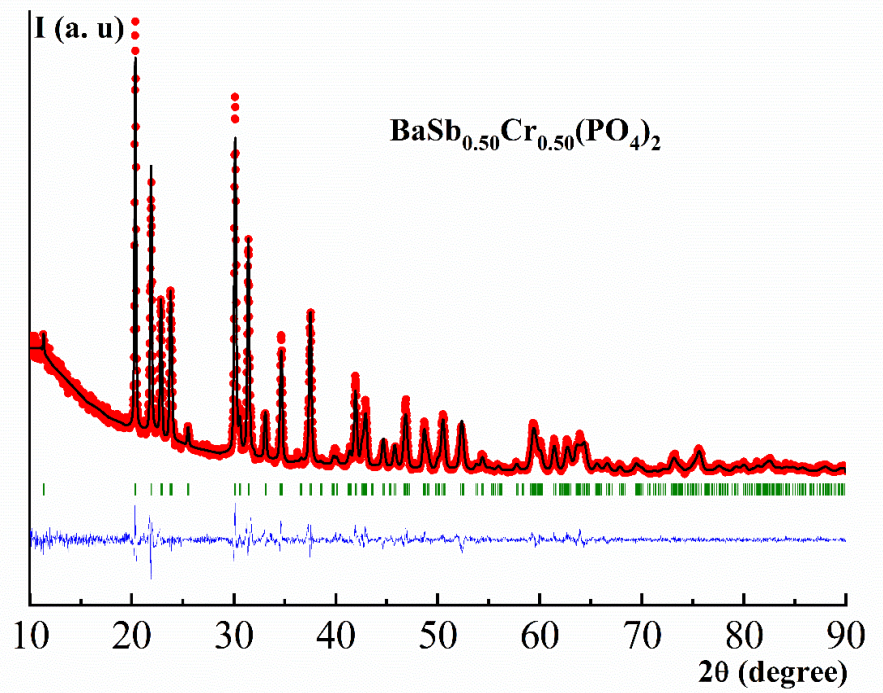


**Figure 1.** Experimental (••••) calculated (——), and difference (——) profile of the XRD patterns of $Ba(Sb_{0.5}Cr_{0.5})(PO_4)_2$

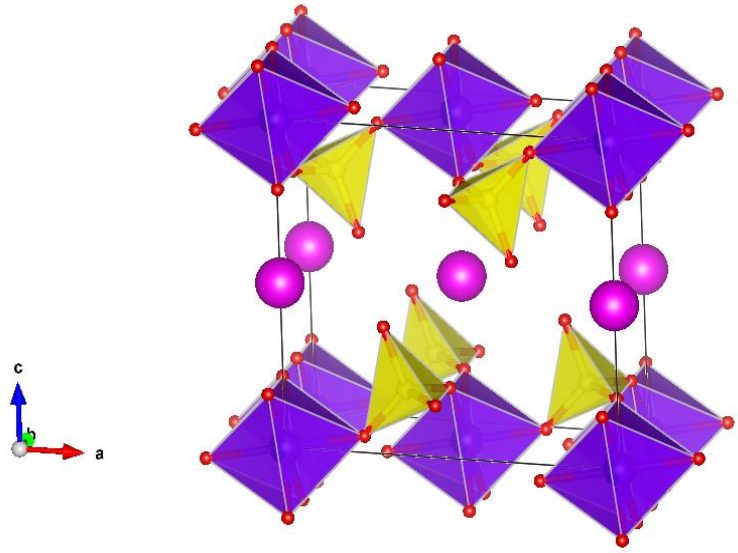


**Figure 2.** Schematic view of the $Ba(Sb_{0.5}Cr_{0.5})(PO_4)_2$ showing Ba atoms, $Sb(Cr)O_6$ octahedra and $PO_4$ tetrahedra

The main distances values of [BaSbCr] are reported in Table 2. The analysis of Ba-O distances values, within $BaO_{10}$ polyhedra, shows that they can be considered as formed by six slightly shortest values ranging from 2.695(6) to 2.767(4) Å and four longer one with an average value of 3.123(3) Å. Thus, the coordination of barium cations can be regarded as 6+4 type. Obtained Sb(Cr)-O bond distances values are comparable to those found for other antimony and chromium phosphate. Mean P–O bond lengths value (i.e.,1.55(1) Å) is fairly regular, and in good agreement with those usually found in the

yavapaiite-type phases [3,18,33]. For more structural information, the bonds valence sums (*BVS*) were calculated from Brown's method [37]. Calculated values for Ba, Cr, Sb, and P are relatively compatible with their oxidation state in $Ba(Sb_{0.5}Cr_{0.5})(PO_4)_2$ (Table 2). X-ray data, collected from the ''observed intensities'' of the Rietveld refinement (CuK$\alpha$1 : 1.5406 Å), of [BaSbCr] compound, are listed in Table 3.

**Table 2.** Selected interatomic distances (Å) and calculated Bond Valence Sum (*BVS*) for $Ba(Sb_{0.5}Cr_{0.5})(PO_4)_2$.

| **$BaSb_{0.5}Cr_{0.5}(PO_4)_2$** | | |
|---|---|---|
| **Sb(Cr)-O distances (Å)**<br>2×Sb(Cr)-O(2) = 1.950(4)<br>4×Sb(Cr)-O(3) = 1.971 (5)<br>Aver.<Sb(Cr)-O> = 1.96(1)<br><br>**Bond Valence Sums (*BVS*)**<br>*BVS*(Sb(Cr)) = 4.4 (should be 4) | **P-O distances (Å)**<br>P-O(1) = 1.520 (5)<br>P-O(2) = 1.568 (4)<br>2×P-O(3) = 1.571 (7)<br>Aver. <P-O> = 1.55(1)<br><br>*BVS* (P) = 4.8 | **Ba-O distances (Å)**<br>2×Ba-O(1) = 2.695(5)<br>4×Ba-O(3) = 2.767 (4)<br>4×Ba-O(1) = 3.123(3)<br>Aver. <Ba-O> = 2.90(1)<br><br>*BVS* (Ba) = 1.9 |

**Table 3**. Powder diffraction data of $Ba(Sb_{0.5}Cr_{0.5})(PO_4)_2$ compound. Diffraction lines with $I_{obs}$< 1 are omitted (Cu$K\alpha_1$; $\lambda$ = 1.5406 Å).

| **$Ba(Sb_{0.50}Cr_{0.50})(PO_4)_2$** | | | | | | | |
|---|---|---|---|---|---|---|---|
| *hkl* | $d_{obs}$ (Å) | 100 $I/I_0$ (obs.) | 100 $I/I_0$ (cal.) | *Hkl* | $d_{obs}$ (Å) | 100 $I/I_0$ (obs.) | 100 $I/I_0$ (cal.) |
| 001 | 7.7794 | 5 | 5 | 312 | 1.9819 | 4 | 5 |
| 110 | 4.3634 | 100 | 96 | 004 | 1.9448 | 7 | 8 |
| 200 | 4.0582 | 61 | 64 | -222 | 1.9371 | 16 | 12 |
| 002 | 3.8897 | 33 | 33 | 222 | 1.8703 | 11 | 9 |
| -111 | 3.8742 | 20 | 19 | -402 | 1.8583 | 4 | 4 |
| 111 | 3.7405 | 37 | 36 | -313 | 1.8231 | 3 | 2 |
| -201 | 3.7165 | 23 | 2 2 | -204 | 1.8086 | 12 | 11 |
| 201 | 3.4902 | 6 | 5 | -114 | 1.8042 | 13 | 12 |
| -112 | 2.9647 | 87 | 77 | 114 | 1.7498 | 10 | 10 |
| -202 | 2.9220 | 10 | 9 | 402 | 1.7451 | 9 | 11 |
| 112 | 2.8459 | 54 | 53 | 130 | 1.6872 | 4 | 3 |
| 202 | 2.7066 | 11 | 11 | 131 | 1.6435 | 1 | 1 |
| 003 | 2.5931 | 23 | 22 | 420 | 1.5967 | 2 | 1 |
| 020 | 2.5874 | 30 | 26 | -314 | 1.5631 | 4 | 3 |
| 310 | 2.3976 | 35 | 36 | -132 | 1.5568 | 11 | 10 |
| -311 | 2.3362 | 1 | 1 | 024 | 1.5546 | 11 | 10 |
| -203 | 2.2651 | 3 | 2 | 510 | 1.5489 | 7 | 7 |
| 311 | 2.2487 | 2 | 2 | 132 | 1.5390 | 6 | 4 |
| 220 | 2.1817 | 4 | 3 | -422 | 1.5093 | 8 | 5 |
| 022 | 2.1543 | 21 | 18 | -224 | 1.4823 | 7 | 5 |
| -221 | 2.1235 | 6 | 5 | -512 | 1.4765 | 3 | 2 |
| 203 | 2.1130 | 8 | 9 | 314 | 1.4627 | 3 | 3 |
| -312 | 2.1057 | 16 | 12 | -404 | 1.4610 | 5 | 4 |
| 400 | 2.0291 | 5 | 6 | | | | |

### 3.2. Rietveld refinement and structural description of $A(Sb_{0.5}Cr_{0.5})(PO_4)_2$ (A = Sr, Pb) phases

The Rietveld refinement in Profil Matching of lead and strontium phases with the previous structural model (i.e., *C2/m* space group and Z = 2) leads to high-reliability factors. Furthermore, several small XRD diffraction lines (e.g., at $2\theta \sim 18.17°$ and 28.33° for [PbSbCr]) remain unindexed, which appeared as the $h+l=2n+1$ superstructure reflections of the *C2/c* doubled cell comparable to the $Pb(Fe_{0.5}Sb_{0.5})(PO_4)_2$ material reported by Aatiq et al. [33]. It is of interest to note that the rotation of the oxygen atoms around their coordination polyhedra is the force driving for the crystal lattice distortion of [ASbCr] (A = Sr, Pb) concerning that of [BaSbCr]. Indeed, these alternating rotations of oxygen atoms cause a doubling of the crystal lattice and consequently lead to the appearance of superstructure lines in the [ASbCr] (A = Sr, Pb) X-ray powder diffraction spectra. Note that about the International Tables for Crystallography data, the *C2/c* (Z=4) is a subgroup of the *C2/m* (Z=2) [38], so the apparent relationship of the lattices and structures between the true (T.Y) (i.e., [BaSbCr]) and the distorted (D.Y) (i.e., [ASbCr] (A = Pb, Sr)) the

following vectorial equations link yavapaiite forms: $a_{(D.Y)} = 2c_{(T.Y)}$; $b_{(D.Y)} = b_{(T.Y)}$; $c_{(D.Y)} = a_{(T.Y)}$.

Thus, the structural model suggested for [PbFeSb] [33] was chosen as starting model for the Rietveld refinement, with the following distribution for the atomic positions: $A^{II}$ (A = Pb, Sr) in 4e (0, -y, 3/4), Sb(Cr) in 4c (1/4, 1/4, 0) and P, O(1), O(2), O(3) and O(4) in 8f (x, y, z) positions. Structural refinement using the aforementioned model gives rise to satisfactory results. Good agreements between the experimental and calculated patterns are seen in Figure 3. The structural data are reported in Tables 4 and 5 for [SrSbCr] and [PbSbCr], respectively.

Given that the structures of $A^{II}(Sb_{0.5}Cr_{0.5})(PO_4)_2$ ($A^{II}$ = Sr, Pb) phases are comparable, we have select to describe only the structure of [PbSbCr].

**Table 4.** Crystallographic data of $Sr(Sb_{0.5}Cr_{0.5})(PO_4)_2$ (*C2/c* space group, Z =4).

**$SrSb_{0.5}Cr_{0.5}(PO_4)_2$**

Space group, *C2/c* (N°15); [Z = 4; a= 16.5038 (2) Å; b= 5.1632(1) Å c= 8.0410(1) Å; β = 115.85(1)°; V = 617(1) Å$^3$]
Experimental data
Temperature, 25 °C; angular range, 10° ≤ 2$\theta$≤ 90°;
step scan increment (2$\theta$) : 0.00836°
Zero-point (2$\theta$), -0.0150 (2)°
Profile parameters
Pseudo-Voigt function, PV = ηL + (1-η)G; η = 0.4348(3)
Half-width parameters, U = 0.3918(2), V = -0.1768(2), and W = 0.0365(1)
Conventional Rietveld R-factors, $R_{WP}$ = 7.8%; $R_P$ = 5.7%; $R_B$ = 4.6%; $R_F$ = 2.7%

| Atom | Site | Wyckoff positions | | | $B_{iso}$(Å$^2$) | Occupancy |
|---|---|---|---|---|---|---|
| **Sr** | 4e | 0 | 0.2916(6) | 0.75 | 2.1(9) | 1 |
| **Sb(Cr)** | 4c | 0.25 | 0.25 | 0 | 1.0(7) | 0.5/0.5 |
| **P** | 8f | 0.1410(2) | 0.7561(6) | 0.7561(3) | 0.9(9) | 1 |
| **O(1)** | 8f | 0.1419(7) | 1.0124(5) | 0.8464(1) | 0.8(1) | 1 |
| **O(2)** | 8f | 0.1551(6) | 0.5412(5) | 0.8940(4) | 1.8(1) | 1 |
| **O(3)** | 8f | 0.2217(3) | 0.7779(2) | 0.7161(8) | 1.8(1) | 1 |
| **O(4)** | 8f | 0.0482(3) | 0.7265(2) | 0.5982(7) | 1.8(1) | 1 |

**Table 5.** Crystallographic data of $Pb(Sb_{0.5}Cr_{0.5})(PO_4)_2$ (*C2/c* space group, Z =4).

**$PbSb_{0.5}Cr_{0.5}(PO_4)_2$**

Space group, *C2/c* (N°15); [Z = 4; a= 16.684 (2) Å; b= 5.156(1) Å c= 8.115(1) Å; β = 115.35(1) °; V = 631(1) Å$^3$]
Experimental data
Temperature, 25 °C; angular range, 10° ≤ 2$\theta$≤ 90°;
step scan increment (2$\theta$) : 0.0167°
Zero-point (2$\theta$), -0.0144 (6)°
Profile parameters
Pseudo-Voigt function, PV = ηL + (1-η)G; η = 0.344(4)
Half-width parameters, U = 0.204(1), V = -0.0385(1), and W = 0.0117(1)
Conventional Rietveld R-factors, $R_{WP}$ = 8.7%; $R_P$ = 6.5%; $R_B$ = 4.5%; $R_F$ = 3.3%

| Atom | Site | Wyckoff positions | | | $B_{iso}$(Å$^2$) | Occupancy |
|---|---|---|---|---|---|---|
| **Pb** | 4e | 0 | 0.3140(4) | 0.75 | 4.5 | 1 |
| **Sb(Cr)** | 4c | 0.25 | 0.25 | 0 | 2.6(1) | 0.5/0.5 |
| **P** | 8f | 0.1461(3) | 0.7569( 6) | 0.7597(8) | 2.5(5) | 1 |
| **O(1)** | 8f | 0.1473(6) | 1.0154(2) | 0.8690(2) | 3.0(1) | 1 |
| **O(2)** | 8f | 0.1640(6) | 0.5464(2) | 0.9036(8) | 2.0(1) | 1 |
| **O(3)** | 8f | 0.2245(7) | 0.7708(3) | 0.7065(7) | 2.0(1) | 1 |
| **O(4)** | 8f | 0.0485(4) | 0.7287(2 ) | 0.6155(6) | 2.0(1) | 1 |

Indeed, the crystal structure can be considered as composed of an alternation of anionic $[(Sb_{0.5}Cr_{0.5})(PO_4)_2]^{2-}$ sheets running parallel to (bc) plane built up of corner-linked $Sb(Cr)O_6$ octaherda and $PO_4$ tetrahedra. While the $Pb^{II+}$ cationic sheets are located amongst $[(Sb_{0.5}Cr_{0.5})(PO_4)_2]^{2-}$ and join them through columbic interactions between the $Pb^{II+}$ and $O^{II-}$ ions to create the 3D framework of [PbSbCr] (Figures 4a and 4b). The lead atom is surrounded by ten oxygen atoms belonging to six $PO_4$ groups. Six vertices of different $PO_4$ groups octahedrally coordinate each Sb(Cr)O6. In such a

way, each $PO_4$ tetrahedra is vertex-connected to three $Sb(Cr)O_6$ octahedra; the remaining unshared oxygen atoms of each tetrahedron has one vertex points into the interlayer where the $Pb^{II+}$ cation takes place. Even though [ASbCr] (A = Sr, Pb) compounds crystallize in the *C2/c* space group, and its a-axis parameter is double compared to that of [BaSbCr] (*C2/m* space group, Z=2), the crystal structure of the three compounds has a similar 3D network.

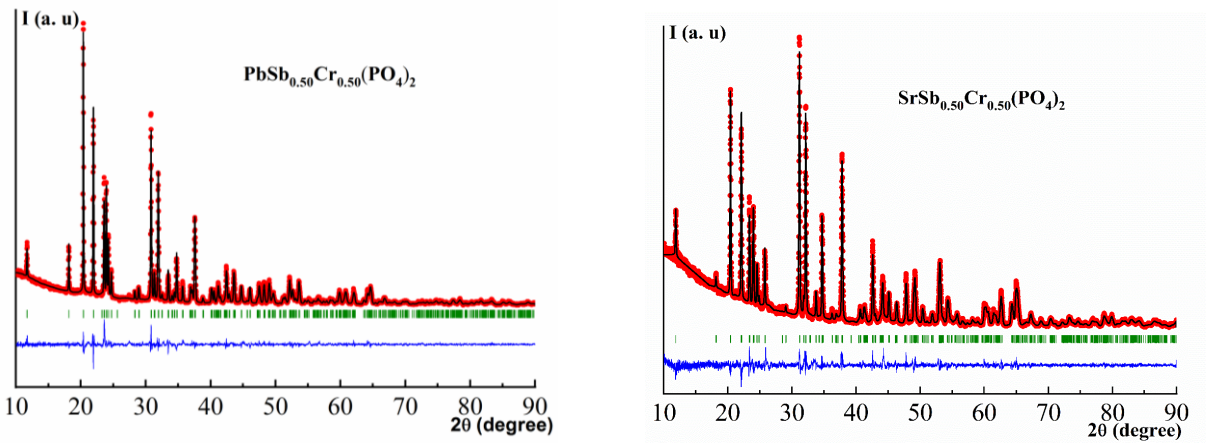


**Figure 3.** Experimental (••••) calculated (——), and difference (——) profile of the XRD patterns of $A^{II}(Sb_{0.5}Cr_{0.5})(PO_4)_2$ ($A^{II}$ = Sr, Pb)

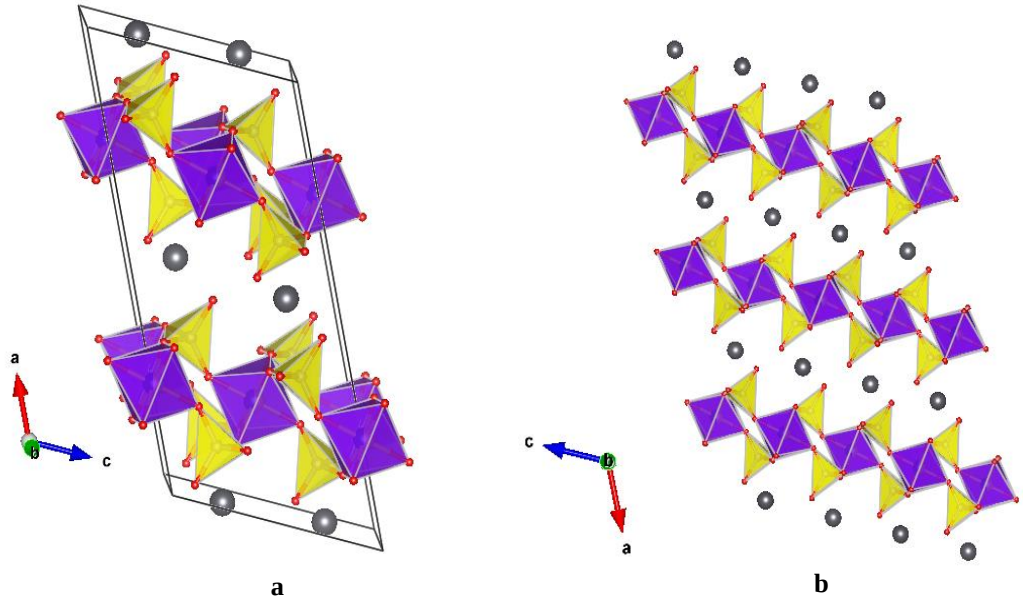


**Figure 4.** (a) View of the structure of $Pb(Sb_{0.5}Cr_{0.5})(PO_4)_2$ showing Pb atoms, $Sb(Cr)O_6$ octahedra and $PO_4$ tetrahedra; (b) Projection in (ac) plane

**Table 6.** Selected interatomic distances (Å) and calculated Bond Valence Sum (*BVS*) for $Sr(Sb_{0.5}Cr_{0.5})(PO_4)_2$.

| **$SrSb_{0.5}Cr_{0.5}(PO_4)_2$** | | |
|---|---|---|
| Sb(Cr)-O distances (Å)<br>2×Sb(Cr)-O(1) = 2.071(4)<br>2×Sb(Cr)-O(2) = 2.067 (5)<br>2×Sb(Cr)-O(3) = 1.992(5)<br>Aver.<Sb(Fe)-O> = 2.04(1) | **P-O distances (Å)**<br>P-O(1) = 1.510(5)<br>P-O(2) = 1.513(4)<br>P-O(3) = 1.504(5)<br>P-O(4) = 1.512(5)<br>Aver. <P-O> = 1.51(1) | **Sr-O distances (Å)**<br>2×Sr-O(1) = 2.583(3)<br>2×Sr-O(2) = 2.658(3)<br>2×Sr-O(4) = 2.569(3)<br>2×Sr-O(4) = 2.849(3)<br>2×Sr-O(4) = 3.412(3)<br>Aver. <Sr-O> = 2.81(2) |
| **Bond Valence Sums (*BVS*)**<br>*BVS*(Sb(Cr)) = 3.6<br>(should be 4) | *BVS* (P) = 5.3 | *BVS* (Sr) = 1.9 |

**Table 7**. Selected interatomic distances (Å) and calculated Bond Valence Sum (*BVS*) for $Pb(Sb_{0.5}Cr_{0.5})(PO_4)_2$.

| **$PbSb_{0.5}Cr_{0.5}(PO_4)_2$** | | |
|---|---|---|
| **Sb(Cr)-O distances (Å)**<br>2×Sb(Cr)-O(1) = 1.993(5)<br>2×Sb(Cr)-O(2) = 2.010(5)<br>2×Sb(Cr)-O(3) = 1.900 (4)<br>Aver.<Sb(Cr)-O> = 1.97(1)<br><br>**Bond Valence Sums (BVS)**<br>***BVS*(Sb(Cr)) = 4.3 (should be 4)** | **P-O distances (Å)**<br>P-O(1) = 1.594(6)<br>P-O(2) = 1.528(6)<br>P-O(3) = 1.544(5)<br>P-O(4) = 1.553(5)<br>Aver. <P-O> = 1.55(1)<br><br>*BVS* (P) = 4.8 | **Pb-O distances (Å)**<br>2×Pb-O(1) = 2.700(6)<br>2×Pb-O(2) = 2.733(6)<br>2×Pb-O(4) = 2.692 (6)<br>2×Pb-O(4) = 2.710 (5)<br>2×Pb-O(4) = 3.443(5)<br>Aver. <Pb-O> = 2.86(1)<br><br>*BVS* (Pb) = 1.7 |

**Table 8**. Powder diffraction data of $Sr(Sb_{0.5}Cr_{0.5})(PO_4)_2$ compound. Diffraction lines with $I_{obs}$< 1 are omitted (Cu$K\alpha_1$; $\lambda$ = 1.5406 Å).

| **$Sr(Sb_{0.5}Cr_{0.5})(PO_4)_2$** | | | | | | | |
|---|---|---|---|---|---|---|---|
| ***hkl*** | $d_{obs}$ (Å) | 100 $I/I_0$ (obs.) | 100 $I/I_0$ (cal.) | *hkl* | $d_{obs}$ (Å) | 100 $I/I_0$ (obs.) | 100 $I/I_0$ (cal.) |
| 2 0 0 | 7.4256 | 15 | 16 | 0 0 4 | 1.8090 | 5 | 5 |
| 1 1 0 | 4.8769 | 5 | 3 | 6 2 0 | 1.7867 | 1 | 1 |
| -1 1 1 | 4.3426 | 74 | 72 | 0 2 3 | 1.7624 | 3 | 3 |
| -2 0 2 | 4.0141 | 58 | 64 | 3 1 3 | 1.7588 | 4 | 4 |
| 1 1 1 | 3.7997 | 36 | 29 | 7 1 1 | 1.7262 | 15 | 16 |
| 4 0 0 | 3.7128 | 20 | 20 | -8 0 4 | 1.7252 | 19 | 20 |
| -3 1 1 | 3.6996 | 33 | 33 | 6 0 2 | 1.7225 | 14 | 12 |
| 0 0 2 | 3.6179 | 14 | 14 | -6 2 3 | 1.7174 | 11 | 8 |
| 3 1 0 | 3.5733 | 5 | 3 | 1 3 0 | 1.7096 | 2 | 2 |
| -4 0 2 | 3.4503 | 19 | 19 | -9 1 1 | 1.6884 | 6 | 7 |
| -3 1 2 | 3.0713 | 3 | 3 | -1 3 1 | 1.6828 | 6 | 6 |
| 3 1 1 | 2.8657 | 100 | 100 | 4 2 2 | 1.6577 | 2 | 2 |
| 2 0 2 | 2.8060 | 9 | 5 | -10 0 2 | 1.6497 | 3 | 2 |
| -5 1 1 | 2.7802 | 76 | 73 | 1 3 1 | 1.6454 | 4 | 4 |
| -6 0 2 | 2.6518 | 8 | 9 | 1 1 4 | 1.6220 | 2 | 1 |
| 0 2 0 | 2.5816 | 36 | 36 | 2 0 4 | 1.6040 | 2 | 2 |
| 5 1 0 | 2.5746 | 24 | 23 | 2 2 3 | 1.6038 | 1 | 1 |
| 6 0 0 | 2.4752 | 4 | 2 | -8 2 1 | 1.5924 | 2 | 1 |
| 0 2 1 | 2.4315 | 3 | 1 | -4 2 4 | 1.5845 | 2 | 2 |
| -3 1 3 | 2.3759 | 60 | 57 | -1 3 2 | 1.5766 | 2 | 2 |
| 2 2 1 | 2.2167 | 6 | 4 | -3 3 2 | 1.5692 | 1 | 1 |
| -4 2 1 | 2.1863 | 6 | 4 | -2 2 4 | 1.5640 | 3 | 2 |
| 5 1 1 | 2.1793 | 5 | 4 | 3 3 1 | 1.5396 | 9 | 5 |
| -2 2 2 | 2.1713 | 2 | 2 | -5 1 5 | 1.5332 | 7 | 6 |
| 4 2 0 | 2.1196 | 28 | 22 | -5 3 1 | 1.5259 | 5 | 5 |
| 0 2 2 | 2.1015 | 5 | 2 | 8 2 0 | 1.5072 | 5 | 4 |
| -4 2 2 | 2.0671 | 2 | 2 | 5 1 3 | 1.4999 | 5 | 3 |
| -8 0 2 | 2.0555 | 4 | 4 | -7 1 5 | 1.4857 | 12 | 10 |
| 1 1 3 | 2.0485 | 16 | 12 | 10 0 0 | 1.4851 | 5 | 5 |
| -4 0 4 | 2.0070 | 8 | 9 | 0 2 4 | 1.4815 | 11 | 10 |
| -7 1 3 | 1.9570 | 5 | 6 | -3 3 3 | 1.4475 | 7 | 7 |
| 4 2 1 | 1.9099 | 2 | 2 | -1 1 5 | 1.4450 | 7 | 7 |
| 2 2 2 | 1.8999 | 17 | 13 | -8 2 4 | 1.4344 | 15 | 13 |
| 8 0 0 | 1.8564 | 11 | 11 | 6 2 2 | 1.4329 | 10 | 10 |
| -6 2 2 | 1.8498 | 20 | 17 | -11 1 3 | 1.4284 | 9 | 10 |
| -5 1 4 | 1.8440 | 9 | 7 | 3 3 2 | 1.4093 | 1 | 1 |
| -4 2 3 | 1.8347 | 2 | 2 | | | | |

The main interatomic distances are listed in Tables 6 and 7 for [SrSbCr] and [PbSbCr], respectively. The $A^{II+}$-O ($A^{II+}$ = Sr, Pb) distances in the $AO_{10}$ polyhedra of both phases indicate that eight oxygen anions surround the AII cation with typical distances values ranging from 2.569(3) to 2.849(3) Å for [SrSbCr]. In the 2.692(6)-2.733(6) Å values range for [PbSbCr]. The two other $A^{II+}$-O distance values

are relatively high (i.e., 3.412(3) Å for Sr-O distances and 3.443(5) Å for Pb-O ones) (Tables 6 and 7). Therefore, the coordination of lead and strontium atoms in both phases can be considered as 8+2 type. In both phases, the $A^{II+}$-O (A = Sr, Pb) distances values are comparable to those already reported for $PbTi(PO_4)_2$ [2] and $SrTi(PO_4)_2$ [24] phases. Sb(Cr)-O bond lengths within $Sb(Cr)O_6$ octahedra range between 1.900(8) and 2.071(9) Å for both compounds. Obtained values are compatible with those calculated from the ionic radii of $Sb^{V+}$ and $Cr^{III+}$ cations in six coordination (Tables 6 and 7). In the case of $PO_4$ tetrahedra, obtained P-O bond distances for both [ASbCr] ($A^{II+}$ = Sr, Pb) are comparable to those generally observed in orthophosphates. Bonds valence sums (*BVS*) calculated from Brown's method [37], indicated that lead, strontium, antimony, chromium, and phosphorus atoms are compatible with their expected oxidation state (i.e., $Pb^{II+}$, Sr $^{II+}$, ($Cr^{III+}$, $Sb^{V+}$) and $P^{V+}$). X-ray data, collected from the ''observed intensities'' of the Rietveld refinement (CuK$\alpha$1: 1.5406 Å), for [SrSbCr] compound, as a selected example, are listed in Table 8.

### 3.3. Infrared and Raman vibrational study

Infrared and Raman spectra of [BaSbCr] and [PbSbCr] are shown in Figures 5(a) and 5(b) respectively. According to literature data of phosphates with yavapaiite phases [33,34,39], bands related to $PO_4$ unit, in $A(Sb_{0.5}Cr_{0.5})(PO_4)_2$ ($A^{II+}$ = Ba, Pb), are relatively strong compared to that of Sb(Cr)-O one within $Sb(Cr)O_6$ octahedra. Thus, assignment of the four ($\nu_1$, $\nu_2$, $\nu_3$, and $\nu_4$) $PO_4$ modes will take these last remarks into account. Note that in [ASbCr] (A = Ba, Pb) materials, P–O distances vary between 1.52 and 1.59 Å with a mean P–O distance of 1.55 Å. Popovic et al. have formulated the following empirical relation [$\nu_{(P\text{-}O)}$ ($cm^{-1}$) = 224500 exp(-*R*/28.35)], which connects P–O bond lengths and stretching frequencies where *R* is the P–O bond lengths in Picometer (pm) [40]. By replacing obtained P-O distance values in the above expression, the calculated frequencies values corresponding to both phosphates are ranging between 850 and 1060 $cm^{-1}$. These last values are relatively in agreement with those observed experimentally, between 865 and 1073 $cm^{-1}$ in the IR and Raman spectra (Figure 5). Thus the symmetric non-degenerate PO stretching modes ($\nu_{1(P\text{-}O)}$) can be assigned to bands ranging between 860-990 $cm^{-1}$ while antisymmetric and doubly degenerate PO stretching ($\nu_{3(P\text{-}O)}$) are located in the 1006-1073 $cm^{-1}$ range. However, the possibility of coupling between $\nu_{1(P\text{-}O)}$ and $\nu_{3(P\text{-}O)}$ stretching bands, around 1000 $cm^{-1}$, cannot be excluded. Bands existing between 400 and 497 $cm^{-1}$ are attributed to the symmetric, triply degenerate OPO bending ($\nu_{2(OPO)}$) modes. In contrast, those ranging between 530-615 $cm^{-1}$ are attributed to the triply degenerate, antisymmetric, and harmonic OPO bending ($\nu_{4(OPO)}$). The bands detected between 646 and 668 $cm^{-1}$ in IR and Raman spectra of both compounds can be associated with the stretching Sb-O vibrations. Similar Sb-O vibrations are already found around 650 $cm^{-1}$ for $AFe_{0.5}Sb_{0.5}(PO_4)_2$(A = Sr, Pb) [33], at 630 $cm^{-1}$ for $Sr_{0.50}SbFe(PO_4)_3$ and $SrSb_{0.50}Fe_{1.50}(PO_4)_3$ phases [27] and around 640 $cm^{-1}$ for $Mn_{0.5}MSb(PO_4)_3$ (M = Al, Fe, Cr) [41] and $M_{0.5}SbFe(PO_4)_3$ (M = Mg, Ni) [42]. The Raman bands observed at 366 $cm^{-1}$ could be assigned to $Cr^{3+}$-O stretching modes of vibrations similar to those observed around 350 $cm^{-1}$ for $Cr^{3+}$-O stretching modes in $Na_3Cr_2(PO_4)_3$ [43]. In low-frequency modes and more precisely for values below 270 $cm^{-1}$, the translational modes of $A^{2+}$ (A = Sr, Pb), $Cr^{3+}$, and $Sb^{5+}$ ions, as well as vibrational modes of $PO_4$, $CrO_6$, and $SbO_6$ groups, should be expected.

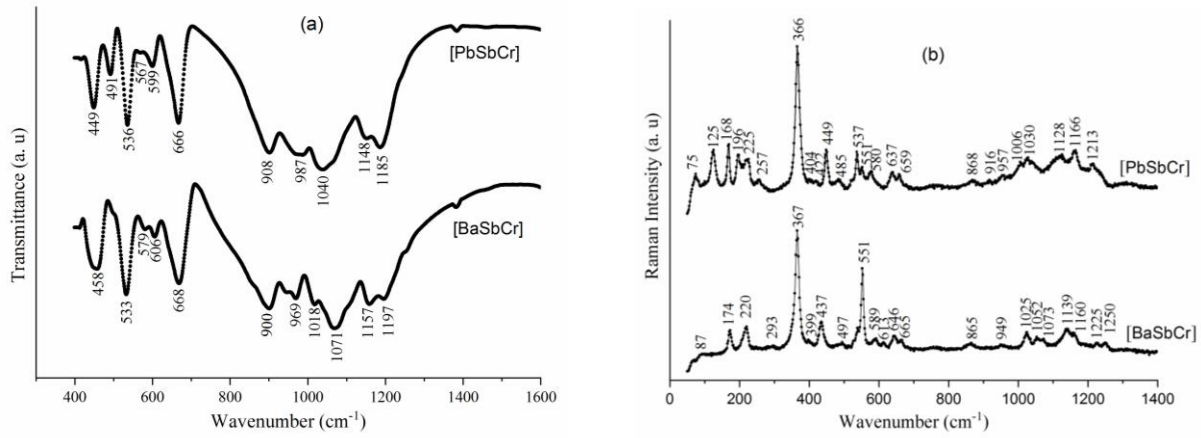


**Figure 5.** Infrared (a) and Raman (b) spectra of $A^{II}(Sb_{0.5}Cr_{0.5})(PO_4)_2$ ($A^{II}$ = Ba, Pb) phases

## 4. Conclusion

In the present work, the crystal structure of the three new $A^{II}(Sb_{0.5}Cr_{0.5})(PO_4)_2$ ($A^{II}$ = Ba, Sr, Pb) compounds have been determined. The results of the Rietveld refinement show that $Ba(Sb_{0.5}Cr_{0.5})(PO_4)_2$ crystallizes in monoclinic system with *C2/m* space

group (Z = 2) while $A^{II}(Sb_{0.5}Cr_{0.5})(PO_4)_2$ ($A^{II}$= Sr, Pb) phases have a monoclinic system with *C*2/*c* space group (Z=4). The three studied compounds crystallize in the yavapaiite-type structure. Even though [ASbCr] (A = Sr, Pb) compounds form in the *C*2/*c* space group and its a-axis parameter is double compared to that found for [BaSbCr], the crystal structure of the three compounds has a similar 3D network. Observed Infrared and Raman bands are assigned according to the vibrations of $Sb(Cr)O_6$ and $PO_4$ polyhedra.

**Acknowledgments**

Financial support of the Moroccan Ministry of Higher Education, Scientific Research and Training of managerial staff (MESRSFC), National Center for Scientific and Technical Research (CNRST) are gratefully acknowledged.

**References**

1- G. Blasse, G.J. Dirksen, The luminescence of barium titanium phosphate $BaTi(PO_4)_2$, Chem. Phys. Lett., **1979**, 62, 19–20.
2- W.L. Zhang, C.S. Lin, Z.Z. He, H. Zhang, Z.Z. Luo, W.D. Cheng, Syntheses of three members of $A(II)M(IV)(PO_4)_2$: luminescence properties of $PbGe(PO_4)_2$ and its $Eu^{3+}$-doped powders, Cryst. En. Comm., **2013**, 15, 7089–7094.
3- D. Zhao, F.X. Ma, H. Yang, W. Wei, Y.C. Fan, L. Zhang, X. Xin, Structure twinning, electronic and photoluminescence properties of yavapaiite-type orthophosphate $BaTi(PO_4)_2$, J. Phys. Chem. Solids, **2016**, 99, 59–65.
4- C.R. Miao, C.C. Torardi, A New High-Efficiency UV-Emitting X-ray Phosphor, $BaHf_{1-x}Zr_x(PO_4)_2$, J. Solid State Chem., **2000**, 155, 229–232.
5- Y. Jiang, L. Wei, C. Xiyu, S. Ge, C. Lixin, G. Rongjie, Synthesis and luminescence of β-$SrGe(PO_4)_2$: RE (RE= $Eu^{2+}$, $Eu^{3+}$, $Tb^{3+}$) phosphors for UV light-emitting diodes, J. Rare Earths, **2017**, 35, 142–148.
6- A.H. Abdeldaim, D.I. Badrtdinov, A.S. Gibbs, P. Manuel, H.C. Walker, M.D. Le, C.H. Wu, D. Wardecki, S.G. Eriksson, Y.O. Kvashnin, others, Large easy-axis anisotropy in the one-dimensional magnet $BaMo(PO_4)_2$, Phys. Rev. B: Condens. Matter., **2019**, 100, 214427.
7- F. Tudorache, K. Popa, L. Mitoseriu, N. Lupu, D. Bregiroux, G. Wallez, Dielectric investigation of $M^{II}M^{IV}(PO_4)_2$ double orthophosphates ($M^{II}$=Ca, Sr, Ba, Pb; $M^{IV}$=Ti, Zr, Hf, Ge, Sn), J. Alloys Compd., **2011**, 509, 9127–9132.
8- K. Popa, R.J. M. Konings, P. Boulet, D. Bouëxière, A.F. Popa, The high-temperature behavior of barium zirconium diorthophosphate, Thermochim. Acta, **2005**, 436, 51–55.
9- K. Popa, R.J.M. Konings, T. Wiss, H. Leiste, Hydrothermal alteration of $Ba_xM^{IV}{}_xCe_{2-2x}(PO_4)_2$ [$M^{IV}$=Zr, Hf] as hosts for minor actinides, J. Radioanal. Nucl. Chem., **2007**, 273, 563–567.
10- S. Neumeier, Y. Arinicheva, Y. Ji, J.M. Heuser, P.M. Kowalski, P. Kegler, H. Schlenz, D. Bosbach, G. Deissmann, New insights into phosphate based materials for the immobilisation of actinides, Radiochim Acta, **2017**, 105, 961–984.
11- A.J. Locock, Crystal chemistry of actinide phosphates and arsenates, In Structural Chemistry of Inorganic Actinide Compounds, Elsevier, **2007**, 217–278.
12- D. Bregiroux, K. Popa, G. Wallez, Crystal chemistry of $M^{II}M^{IV}(PO_4)_2$ double monophosphates, J. Solid State Chem., **2015**, 230, 26–33.
13- N. Clavier, R. Podor, N. Dacheux, Crystal chemistry of the monazite structure, J. Eur. Ceram. Soc., **2011**, 31, 941–976.
14- D. Kitaev, Y.F. Volkov, A. Orlova, Orthophosphates of tetravalent Ce, Th, U, Np, and Pu with the monazite structure, Radiochemistry, **2004**, 46, 211–217.
15- A. Orlova, D. Kitaev, N. Kazantsev, S. Samoilov, V. Kurazhkovskaya, E. Vopilina, Double phosphates of Ce (IV) and some mono-and divalent elements: synthesis and crystal structure, Radiochemistry, **2002**, 44, 326–331.
16- A. Orlova, D. Kitaev, D. Kemenov, M. Orlova, G. Kazantsev, S. Samoilov, V. Kurazhkovskaya, Synthesis and Crystal-Chemical Properties of Phosphates $B^{II}R^{III}M^{IV}(PO_4)_3$ Containing f, d, and Alkaline-Earth Elements, Radiochemistry, **2003**, 45, 103–109.
17- R. Podor, M. Cuney, C.N. Trung, Experimental study of the solid solution between monazite-(La) and $(Ca_{0.5}U_{0.5})PO_4$ at 780 C and 200 MPa, Am. Mineral., **1995**, 80, 1261–1268.
18- K. Fukuda, A. Moriyama, T. Iwata, Crystal structure, phase transition, and anisotropic thermal expansion of barium zirconium diorthophosphate, $BaZr(PO_4)_2$, J. Solid State Chem., **2005**, 178, 2144–2151.
19- K. Popa, D. Bregiroux, R.J.M. Konings, T. Gouder, A.F. Popa, T. Geisler, P.E. Raison, The chemistry of the phosphates of barium and tetravalent cations in the 1:1 stoichiometry, J. Solid State Chem., **2007**, 180, 2346–2355.
20- K. Popa, G. Wallez, D. Bregiroux, P. Loiseau, $M^{II}Ge(PO_4)_2$ (M=Ca, Sr, Ba): Crystal structure, phase transitions and thermal expansion, J. Solid State Chem., **2011**, 184, 2629–2634.
21- A. Leclaire, M. Barel, J. Chardon, B. Raveau, A Mo (IV) monophosphate, $BaMo(PO_4)_2$, with

the yavapaiite layer structure, J. Solid State Chem., **1995**, 116, 364–368.
22- E. Morin, G. Wallez, S. Jaulmes, J.C. Couturier, M. Quarton, Structure of $Pb^{II}Sn^{IV}(PO_4)_2$: Stereochemical Activity of the Lead II Lone Pair, J. Solid State Chem., **1998**, 137, 283–288.
23- K. Fukuda, K. Fukutani, Crystal structure of calcium zirconium diorthophosphate, $CaZr(PO_4)_2$, Powder Diffr., **2003**, 18, 296–300.
24- D. Zhao, H. Zhang, Z. Xie, W.L. Zhang, S.L. Yang, W.D. Cheng, Syntheses, crystal and electronic structures of compounds $AM(PO_4)_2$ (A = Sr, M = Ti, Sn; A = Ba, M = Sn), Dalton Trans., **2009**, 5310–5318.
25- A. Aatiq, R. Hassine, M.R. Tigha, I. Saadoune, Structures of two newly synthesized $A_{0.50}SbFe(PO_4)_3$ (A= Mn, Cd) Nasicon phases, Powder Diffr., **2005**, 20, 33–39.
26- A. Aatiq, M.R. Tigha, R. Hassine, I. Saadoune, Crystallochemistry, and structural studies of two newly $CaSb_{0.50}Fe_{1.50}(PO_4)_3$ and $Ca_{0.50}SbFe(PO_4)_3$ Nasicon phases, Powder Diffr., **2006**, 21, 45–51.
27- A. Aatiq, M.R. Tigha, S. Benmokhtar, Structure, infrared, and Raman spectroscopic studies of new $Sr_{0.50}SbFe(PO_4)_3$ and $SrSb_{0.50}Fe_{1.50}(PO_4)_3$ Nasicon phases, J. Mater. Sci., **2012**, 47, 1354–1364.
28- M. Varma, H. Poswal, S. Velaga, Pressure-induced phase transitions in $BaZr(PO_4)_2$ studied using x-ray diffraction, Raman spectroscopy, and first-principles calculations, J. Appl. Phys., **2020**, 127, 135902.
29- G. Wallez, D. Bregiroux, K. Popa, P.E. Raison, C. Apostolidis, P. Lindqvist-Reis, R.J.M. Konings, A.F. Popa, $BaAn^{IV}(PO_4)_2$ ($An^{IV}$ = Th, Np)-A New Family of Layered Double Phosphates, Eur. J. Inorg. Chem., **2011**, 2011, 110–115.
30- M. Keskar, B.G. Vats, R. Phatak, K. Krishnan, S.K. Sali, S. Kannan, Structural and thermal studies of $SrU(PO_4)_2$ and $BaU(PO_4)_2$, J. Alloys Compd., **2017**, 725, 1199–1209.
31- N. Sarukhanyan, L. Iskhakova, V. Trunov, Crystal structure of $RbEu(SO_4)_2$, Kristallografiya, **1983**, 28, 452-456.
32- K. Popa, G. Wallez, P.E. Raison, D. Bregiroux, C. Apostolidis, P. Lindqvist-Reis, R.J.M. Konings, $SrNp(PO_4)_2$ : an Original Ordered Modification of Cheralite, Inorg. Chem., **2010**, 49, 6904–6908.
33- A. Aatiq, M.R. Tigha, R. Fakhreddine, D. Bregiroux, G. Wallez, Structure, infrared and Raman spectroscopic studies of newly synthetic $A^{II}(Sb^{V}_{0.50}Fe^{III}_{0.50})(PO_4)_2$ (A = Ba, Sr, Pb) phosphates with yavapaiite structure, Solid State Sci., **2016**, 58, 44–54.
34- R. Fakhreddine, A. Aatiq, Structure, Infrared and Raman spectroscopic studies of the new $Ba(Nb^{V}_{0.5}M^{III}_{0.5})(PO_4)_2$ ($M^{III}$ =Al, Cr, Fe, In) yavapaiite compounds 'series, Mediterr. J. Chem., **2019**, 8, 397-408.
35- J. Rodriguez-Carvajal, Collected abstract of powder diffraction meeting, Toulouse Fr, **1990**, 127.
36- T. Roisnel, J. Rodríquez-Carvajal, WinPLOTR: a windows tool for powder diffraction pattern analysis, In Materials Science Forum, Transtec Publications, **1999**, 378, 118–123.
37- I.D. Brown, D. Altermatt, Bond-valence parameters obtained from a systematic analysis of the Inorganic Crystal Structure Database, Acta Crystallogr., Sect. B: Struct. Sci., **1985**, 41, 244–247.
38- T. Hahn, U.Shmueli, J.W. Arthur, International Tables for Crystallography, Vol. A. space-group symmetry, D. Reidel Publ. Co., Dordrecht, Holland/Boston, Crystal Research and Technology, **1984**, 1306.
39- M.T. Paques-Ledent, $A^{II}B^{IV}(XO_4)_2$ phosphates and arsenates with yavapaiite structure I: isostructural relationship and vibrational study, J. Inorg. Nucl. Chem., **1977,** 39, 11–17.
40- L. Popović, D. de Waal, J.C.A. Boeyens, Correlation between Raman wavenumbers and P-O bond lengths in crystalline inorganic phosphates, Journal Raman Spectroscopy, **2005**, 36, 2-11.
41- N. Anantharamulu, K.K. Rao, M. Vithal, G. Prasad, Preparation, characterization, impedance, and thermal expansion studies of $Mn_{0.5}MSb(PO_4)_3$ (M = Al, Fe, and Cr), J. Alloys Compd., **2009**, 479, 684–691.
42- A. Aatiq, A. Marchoud, H. Bellefqih, M.R. Tigha, Structural, and Raman spectroscopic studies of the two $M_{0.50}SbFe(PO_4)_3$ (M= Mg, Ni) NASICON phases, Powder Diffr., **2017**, 32, S40–S51.
43- M. Barj, G. Lucazeau, C. Delmas, Raman, and infrared spectra of some chromium Nasicon-type materials: short-range disorder characterization, J. Solid State Chem., **1992**, 100, 141-150.